Fundamental Issues When Creating an Autonomous Platform for a UWB Navigation System

Damian Grzechca, Krzysztof Tokarz, Krzysztof Hanzel, Sebastian Pokuciński

Faculty of Automatic Control, Electronics and Computer Science
Silesian University of Technology, ul. Akademicka 16.44-100, Gliwice, Poland.
Damian.Grzechca@polsl.pl, Krzysztof.Tokarz@polsl.pl,
Krzysztof.Hanzel@polsl.pl, sebapok553@student.polsl.pl

Abstract: The paper presents some fundamental issues when using a UWB (Ultra Wide Band) navigation system on a fast prototyping platform such as LEGO Mindstorms. The authors present the functional parameters of the chassis and show how it affects the navigation scheme of a UWB positioning system that consisted of four reference points and one tag, which was placed on the vehicle. The chassis was prepared on the Lego Mindstorms platform and the functional parameters such as axle angle, speed and delay were determined. The obtained results indicate that there are chassis limitations for using a UWB positioning system to navigate. The accuracy of reaching the destination point, which was equal to the size of the car that was constructed, was acceptable. The study also enabled us to conclude that this project could be the nucleus of a more complex scenario in smart autonomous robotics or public transport (support for small autonomous vehicles, electric personal transport vehicles, drones, ADAS systems, etc.).

Keywords: autonomous vehicle, positioning, ultrasonic sensor, UWB, Mindstorms platform, IPS

1. INTRODUCTION

In the modern world, more and more emphasis is being placed on automating our lives and creating devices that relieve us of some everyday activities. One of the futuristic concepts is autonomous vehicles, whose preliminary versions can be slowly observed. They use many different technologies, one of them which is positioning – and therefore the possibility of precisely designating the location of each other is quite modest so far. Over the years, IPS (indoor positioning systems) technologies have developed rapidly – currently, dozens of approaches, which specify various divisions because of the technology used, can be mentioned. An example can be the use of low-range systems such as radio-frequency identification (RFID) tags (Ni et al., 2004; Yang et al., 2013), microelectromechanical systems (MEMS) (Grzechca et al., 2017) or inertial measurement units (IMU) (Guo et al., 2015). Wi-Fi (Biswas and Veloso, 2010; Combain Mobile AB, n.d.; Wang et al., 2017) or GSM (Constandache et al., 2010) can be used as GPS-assist systems. Finally, there have been attempts to use various other systems to play the role of independent localization systems such as Bluetooth (Aalto et al., 2004; Cantón et al., 2017; Fischer et al., 2004; Grzechca et al., 2016), Zigbee (Jin et al., 2008; Liu et al., 2017), infrared (Israel and Dehy, 2004), vision systems (Bernardin and Stiefelhagen, 2008; Kato and Billinghurst, 1999; Pescaru and Curiac, 2014), etc. In the outdoor positioning technology (OPS – outdoor positioning systems), GPS technology can be seen the most in various releases (GPS, GLONASS, BEIDOU). Although the use of satellite navigation works well, such a precise positioning of objects for civilian purposes is still difficult and unreliable (Zhao et al., 2016). An example of this are the urban conditions in which positioning systems with GPS technology become unreliable and their precision drastically decreases because they are surrounded by high buildings, varying street widths and unfavourable weather conditions. Navigating robots using GPS and a statistical approach is possible, however, because on a larger scale it enables non-constant local errors to be eliminated, however, it is susceptible to global errors (such as atmospheric and relativistic effects) (Jurisica et al., 2010). The UWB system, which combines the advantages of the known IPS solutions and the universality of OPS, seems to be the answer to these problems. Although it has not been extensively used for positioning objects outside of buildings, a previous work confirmed that the system has sufficient precision (Gezici and Poor, 2009) even when moving at a high speed (Grzechca and Hanzel, 2018). In addition, a UWB-based system would expand the possibilities of the solutions related to, for example, Bluetooth technology (Yu Wooyeon et al., 2015) that are already being used with new capabilities. Based on these observations, we decided to prepare a vehicle model that would work in conjunction with a UWB system, which based on the response from this system in real-time will move to the point that had been selected in the GUI (graphical user interface). As a starting point for vehicle positioning, we decided to use a product from a leading company that produces UWB modules and their DWM1000 modules. Only a few years ago, the accuracy of wireless sensor networks (WSN) using TDOA was measured as 2-3 m (Ilas et al., 2012), while today's WNS, which are based on UWB, have an accuracy of 10 cm at speeds up to 5 m/s (18 km/h) (“ScenSor Module DWM1000 – WSN | DecaWave,”

n.d.). A vehicle equipped with a UWB would also prove itself in the Vehicle Detection Systems because of its resistance to factors such as weather conditions or the time of day, which have a significant impact on current systems (Abdel-Rahim et al., 2018).

To date, several attempts have been made to use constructions for autonomous driving that are based on the Mindstorms platform. The first example is the work (Pinto et al., 2012) in which the authors presented a vehicle that was used to learn the location. The vehicle used orientation sensors such as touch, sound, ultrasound and light. The sensors were, in fact, the weakness of this publication because – as the authors write – IR sensors can only be precise at distances less than or equal to 30 cm. In addition, the authors had to deal with measurement noise, which was a consequence of the methodology that was used. In the next publication (Gesu et al., 2000), the authors used light sensors to determine the route of an autonomous vehicle that was based on the proposed platform. However, they were not able to determine where the obstacle was located, they could only determine that it was in front of the vehicle. The paper (Stevenson and Schwarzmeier, 2007) presented a webcam for all of its navigation. The integration of the camera, a robot and a computer that controlled the vehicle is discussed, however, it must be remembered that the computing power that was required to analyse the image was huge and that it was necessary to provide optimal conditions (the amount of light, the transparency of the air). The LEGO company also offer the possibility of using its bricks for autonomous driving (Education, n.d.), and describes various approaches, for example, for parking with various levels of difficulty. Moreover, mobile robots have already been positioned based on a UWB (Röhrig et al., 2012); however, none of them investigated autonomous driving along a designated route for specific vehicle parameters. Unfortunately, there are chassis limitations in positioning for navigation.

Because no information was found in the literature about the chassis parameters, we decided to prepare a platform that was equipped with a UWB positioning system. The authors wanted to determine the functional parameters that were required for the chassis such as the maximum speed, stop success rate, distance to stop error and turning radius. The last parameter is the delay between the control command and chassis response.

2. CHASSIS CREATION AND PARAMETERS DETERMINATION

2.1 Assumptions

During the first stage, the chassis was built and the functional parameters were determined:

- Maximum vehicle speed – v [m/s],
- Vehicle turning radius – r [m],
- Vehicle distance to stop error – Sd [m],
- Vehicle stop success rate – Sr [%],

All of these parameters affect the algorithms for UWB navigation schemes. In addition, a UWB positioning system has the following limitations:

- UWB sampling frequency – Pf [Hz]
- UWB standard deviation – Pd [m]

During the construction stage, the authors wanted to create a chassis with the following parameters and properties:

- Enable the vehicle to move at speeds greater than or equal to 1 m/s,
- Enable the vehicle to detect objects in front of the car and prevent collisions in 95% of the cases,
- Enable the vehicle to have control precision between the designated distance and the actual one at no more than the vehicle size,
- Make it possible for the vehicle to perform a turning manoeuvre while maintaining a turning circle of less than 2 m

The assumptions that were made were deemed to be sufficient to correctly model the traffic of a vehicle operating in a mixed IPS / OPS environment (e.g. an airport trolley carrying luggage from the arrivals hall to a passengers car).

2.2 Constructing, testing and validating the assumptions.

Because all of the default models that were proposed by the Mindstorms platform manufacturer moved too slowly and were not able to be controlled enough, we decided to construct a new solution.

Achieving the first requirement involved using a gear that multiplied the turnover that was obtained from the engine. When calculating the required transmission ratio of the gear unit that was used, and in the subsequent calculation of the distance that the vehicle would have to travel to each degree of rotation (required for steering), formula (1) was used.

$$s = \frac{\pi * i * d_k}{360°} \tag{1}$$

where s is the distance to be covered by the vehicle, i is the drive ratio and d_k is the diameter of the wheels that were mounted on the car.

In order to meet the first of the requirements, we decided to create a test scenario in which the vehicle would accelerate to 25, 50 and 75% of the engine power, respectively, (each of the tests consisted of ten measurement series), after which its speed would be determined based on an analysis of a time-lapse video (for the 120 fps video and speed of 1 m/s, each 1 frame was equal to 0.83 cm). A route was marked out on which the car in a 1 m area made a free passage and then on the next distance of 60 cm, the car speed was registered. The test showed that for the third of the series of measurements, the vehicle obtained the required speed of at least 1 m/s (exactly 1.1 m/s as is shown in Fig. 1. Based on that result, it can be seen that our v parameter was 1.1 m/s.

To meet the second assumption, ultrasonic sensors were used in order to avoid up to 95% of collisions. Unfortunately, because the producer did not provide the full specifications of the systems, it was necessary to measure the devices first as shown in Fig. 2.

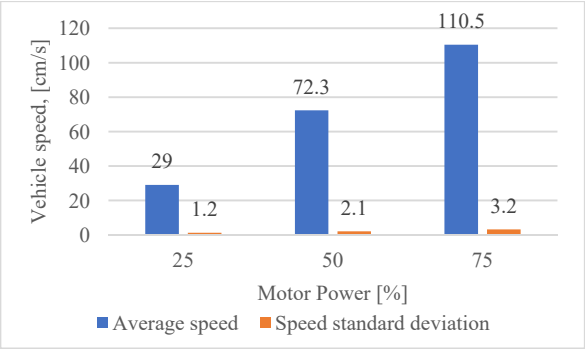

Fig. 1. Diagram of the average and standard deviation of the vehicle speed for the given power of the engine.

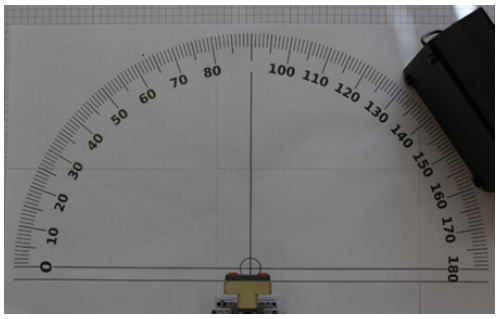

Fig. 2. Picture of the test conditions of the obstacle detection range using an ultrasonic sensor.

Based on the obtained results (Table 1), it can be stated that the factory-fitted sensors fit within the error of the method in the case of the straightforward detection coincided with the expectations (assumed 1cm).

Table 1. Accuracy of the ultrasonic sensor – actual to measured distance difference.

Distance tested	Measured distance	Error
25 cm	23 cm	2 cm
50 cm	49 cm	1 cm
75 cm	74 cm	1 cm

Based on the synthetic measurements alone, it can be said that the distance of the detected objects significantly increased (more than 2.5 times) compared to the solution that was based on the IR sensor in the publication (Pinto et al., 2012). In addition, the detection angles that were obtained were up to 55 degrees in both directions, while the accuracy began to drop above 30 degrees. To minimize this effect, we decided to use three sensors, which significantly widened the viewing angle and made it possible to detect scenarios with different variants of obstacles and their avoidance in a predictable way that was defined by the authors.

In addition, it should be noted that the 30 completed tests all ended with the correct stop of the vehicle. This translated into an Sr parameter value = 100% and an Sd = 0.02 m.

The third requirement was to obtain control precision at an error level of up to 15% (getting the vehicle to the destination with the designated distance to be travelled). To achieve such accuracy, a validation scenario was first designed that included a passage on a straight line. Based on it and using the encoder value that was available on the motor, the control was corrected. The results for the synthetic straight-line travel are shown in Table 2.

Table 2. Accuracy of the start/stop procedure – measuring travelled to the designated distance difference.

Engine power [%]	Distance [cm]		
	25	50	75
25	24,33	49,48	74,87
50	26,76	50,90	75,54
75	30,34	56,84	81,25

The results indicated that for lower speeds the proposed solution reached a value close to expected. For higher speeds, the differences reached as much as 30%, however, this was caused by the vehicle moving along the floor tiles after the wheels were locked while braking and the slip that occurred during a sudden start with full engine power. Indications of the tachometer, however, clearly showed that the distance that was travelled by the circle was 25.56 cm, hence the expected value. In order to minimize the error, it was necessary to enter a parameter that made the movement independent of the surface on which the vehicle moved. After making this correction, the error rate for moving at 75% power, even for a short distance did not exceed 6%, which met the set requirements. The high precision of the system allows the assumption that it will be possible to use it for precise manoeuvres at transhipment sites, transport hubs or parking lots for trucks where economical space management (Bayraktar et al., 2015) is an extremely important element.

Additionally, the indications of the standard deviation of the distances that were travelled that are presented in Table 3 show that the vehicle was moving in a predictable and easy to repeat manner, even in the case of the aforementioned – engine power equal to 75% and a distance of 25 cm. The differences, however, were so small that they permitted us to assume that the error would always be below 1 cm regardless of the speed and distance the vehicle travels.

Table 3. Average distance standard deviation for the start/stop procedures.

Engine power [%]	Distance standard deviation [cm]		
	25	50	75
25	0,46	0,39	0,90
50	0,90	0,74	0,50
75	0,38	0,99	0,54

The last requirement was whether it was possible to perform a turning circle of less than 2 m. The original vehicle, unfortunately, did not meet the required assumptions, especially because the tires locked at high speeds, which would have made it impossible to perform any manoeuvre. In order to comply with this requirement, the car had to be equipped with some of the elements of a McPherson column, including in the steering knuckle. After that modification, the wheels of the car were able to make a rotation even by 39 degrees, as is shown in Fig. 3.

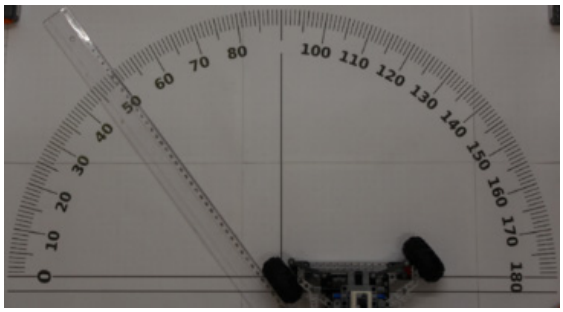

A

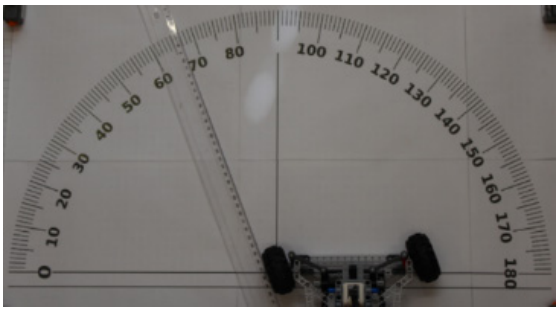

B

Fig. 3. Wheel turning range in the safe A and unsafe B positions.

Based on this and the test runs, two tire deflection angles were determined – one for a low speed (up to 0.7 of v of the vehicle) presented in Figure 3A and one for a high engine power (above 0.7 of the v) – presented in Figure 3B. This was caused by blocking the mechanism at a high speed and a large turn, which forced us to design an algorithm that slowed it down before making a sharp turn.

The vehicle turning radius r, which has to be known, depends on two things:

- The wheelbase – w, which is the distance between the front and rear wheels
- The angle – α of the front wheel

$$r = \frac{w}{tan(\alpha)} \tag{2}$$

Therefore, for a safe speed (39 degrees) r = 0.37 m and for the max speed (23 degrees) r = 0.71 m.

2.3 The UWB system that was used

The specific distances between the nodes were calculated using the travel time of a radio signal and the velocity of the propagation of an electromagnetic wave. The communication process (Kolakowski et al., 2010) is presented in Fig. 4 in simplified form.

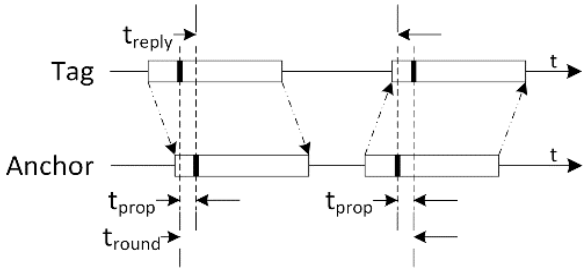

Fig. 4. Communication between a UWB Anchor and Tag.

The obtained wave propagation time – t_{prop} was converted into the distance between the nodes and tag and a specific anchor. The time of flight was calculated using equation (3). When the time of flight was calculated, the distance between the tag and specific anchor could be calculated using equation (4).

$$t_{prop} = \frac{t_{round} - t_{reply}}{2} \tag{3}$$

$$d = c \cdot t_{prop} \tag{4}$$

where d – the distance between the nodes, c – the speed of the electromagnetic wave propagation and t_{prop} – the wave propagation time between the nodes.

Each distance d was received in 16 ms, which gave a Pf value of 62.5 Hz on average. The Pd parameter was determined based on a static measurement for 10,000 samples and was 0.15 m.

The test stand consisted of a UWB tag – a movable device that processed the signals and calculated the distances and four anchors – the stationary reference points as presented in Fig. 5. All of these devices were made of DWM1000 chips, which are manufactured by DecaWave and are compatible with the IEEE802.15.4-2011 standard. According to the manufacturer instructions, a system was designed to create a real-time (RT) IPS, which enabled objects to be localized with a 10 cm accuracy at a maximum moving speed of up to 5 m/s (subject to IPS). This technology also provided high-speed data transmission of up to 6.8 Mb/s ("ScenSor Module DWM1000 – WSN | DecaWave," n.d.). The system that was based on these devices returned the distances between the tag and the anchors in centimetres (using TDoA).

The four anchors defined the coordinate system and the entire test stand was presented as is it was shown on a simplified GUI of the management program (Fig. 6*)*. The reference points (anchors) were placed on the ground (A1-A4), on a 4 m square and the car (C) in this example moved from point to point (P1-P4) in the designated square. In this case, a multilateration algorithm was used that included each of the available reference points. However, for example in the case of greater accessibility, it is also possible to select additional points (Albaidhani et al., 2019).

A

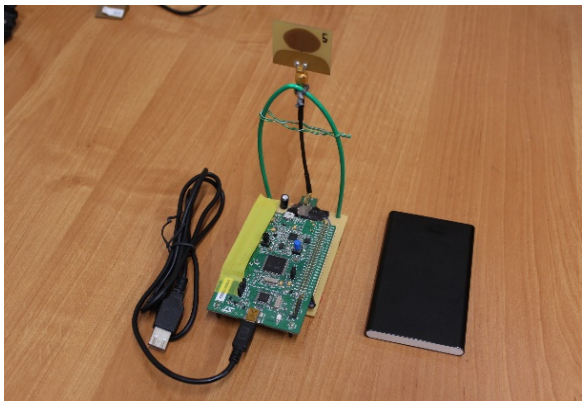

B

Fig. 5. Elements of the UWB localization system. In A, the anchor (hardware of the node in the box) and in B, the hardware of the nodes (DecaWave DWM1000 with an STM32 Microcontroller).

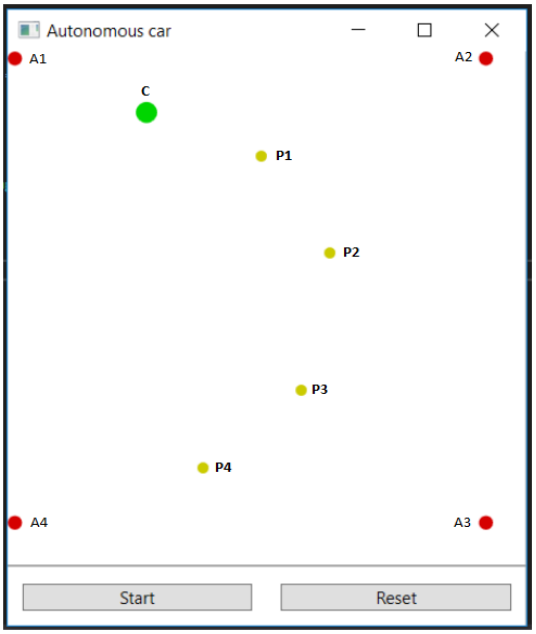

Fig. 6. The four anchors (A1-A4) that defined the coordinate system with the car (C) and path points (P1-P4).

The data processing is presented in the next chapter.

The final version of the chassis, which corresponded to the functional parameters listed above and is shown in Fig. 7, had two servos on the rear axle and one servo on the steering axle. All of the servomotors were connected to an E V3 brick and the control signals were sent *via* Bluetooth. The parameters are listed in Table 4.

Table 4. Selected servo parameters.

Parameter	Medium Servo Motor	Large Servo Motor
Revolutions per minute	240-250	160-170
Running torque	8 N/cm	20 N/cm
Stall torque	12 N/cm	40 N/cm
Tacho feedback	to one degree of accuracy	to one degree of accuracy

A collision avoidance system with three ultrasonic sensors at the front of the vehicle and one IR (Infrared) sensor at the rear was also built. The UWB positioning system tag was embedded on top of the chassis.

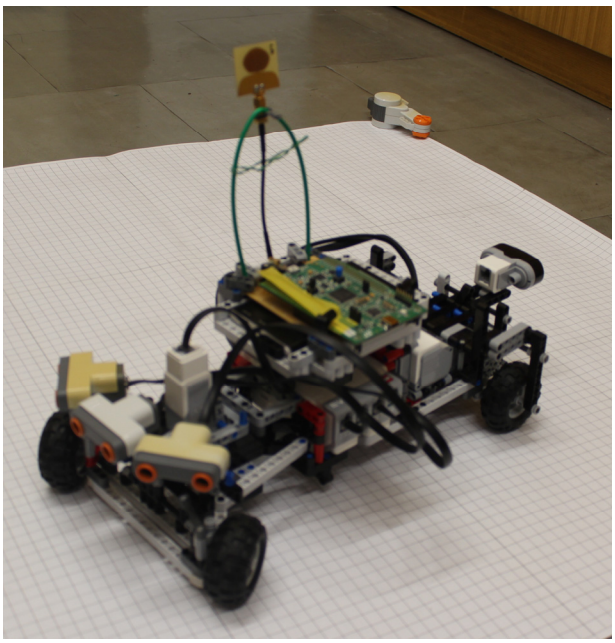

Fig. 7. The chassis that was evaluated.

In conclusion, the platform that was built had the following parameters:

- v = 1.1 m/s
- r = 0.71m – as the maximum value
- Sd = 0.02 m
- Sr = 100 %
- Pf = 62.5 Hz
- Pd = 0.15 m

3. DATA PROCESSING AND POSITION DETERMINATION

Based on the data that was obtained from the reference points, trilateration was performed according to the model presented in (Bucher and Misra, 2002). Initially, the position that was obtained was subjected to simple filtration using two methods with a variable filter window – the median and the moving average. Subsequently, based on previous experience as well as on the low speed of the movement of the tracked object and the high frequency of the acquired data, we decided to use aggregating buckets, which had a positive effect on the data that was obtained from the UWB system. The method was described in the publication (Grzechca et al., 2018). In addition, it was assumed that each point from the aggregating bucket had to be located no further than the value Pd from another. For this purpose, the following patterns were used for the dances that were received (5-6)

$$d = \sum_{n=2}^{\lceil k \rceil} \left(\sqrt{(x_n - x_{n-1})^2 + (y_n - y_{n-1})^2} \right) \quad (5)$$

$$k = \frac{Pf * Pd}{v} \quad (6)$$

where Pf, Pd and v were dependent on the parameters of the vehicle, d was a distance between two points, k was the maximum number of samples that were obtained from the UWB system in a given situation (for one aggregation bucket) and d was the sum of the distances between the points in current bucket that the car travelled.

The points that passed the aggregation bucket stage were applied to the autonomous driving algorithm – this provided us with a regular flow of points and resistance of the algorithm to the UWB system property that resulted from the Pd parameter.

The entire process is shown on the data flowchart in Fig. 8.

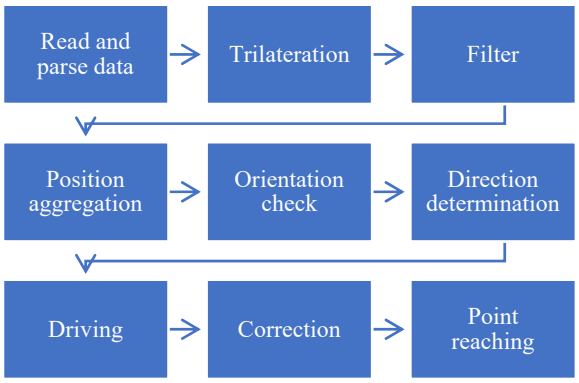

Fig. 8. Data flow during the autonomous driving process.

3.1 Orientation check

During the movement, it was assumed that the vehicle would move in a straight line towards the specified checkpoint. For this purpose, the angle between the vector that was determined based on the historical data and the current point (u) and the target as a (v) was checked using the equations (7-9) as shown in Fig. 9.

$$u \cdot v = \|u\|\|v\| \cos(\alpha) \tag{7}$$

$$\cos(\alpha) = \frac{u \cdot v}{\|u\|\|v\|} \tag{8}$$

$$\alpha = \arccos\left(\frac{u \cdot v}{\|u\|\|v\|}\right) \tag{9}$$

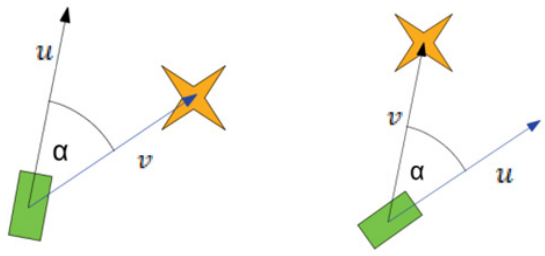

Fig. 9. Detection scheme for the smallest angle α for the turn towards the destination point.

In addition, it was also assumed that the car would go to the target at the smallest possible angle (always less than 180 degrees). For this purpose, an element that was responsible for detecting and correcting the degree of the turn was added to the derived equation (10).

$$\alpha = \arccos\left(\frac{u \cdot v}{\|u\|\|v\|}\right) * sng(u \times v) \tag{10}$$

3.2 Obstacle detection

Based on Fig. 10, it can be stated that three basic scenarios that occurred. The first (in the graphic as A) was the detection of an obstacle on one of the sensors (a blocked path is presented as a vector u). Then, any other path that would guarantee that the destination (v as a possible path vector) would be reached should be selected. The second case when an obstacle was detected on two of the three sensors (in the graphic as B). Information about getting to or following object can be obtained here. It was, therefore, necessary to move towards the empty space in order to avoid collisions. The third, most unfavourable from the point of view of the system was a scenario in which the vehicle was jammed (in the graphic as C). In this case, the vehicle had to be returned to the last known safe position first, and then it took a different route, excluding the one that had been used so far. Using this approach and three sensors, the problem that existed in the publication of (Gesu et al., 2000) in which the obstacle position was not known, but only the information about its existence, which made it difficult to avoid it, was solved. In addition, such a system when used in conjunction with an external positioning system enabled the detected objects to be mapped and included in the next route designation in a given area.

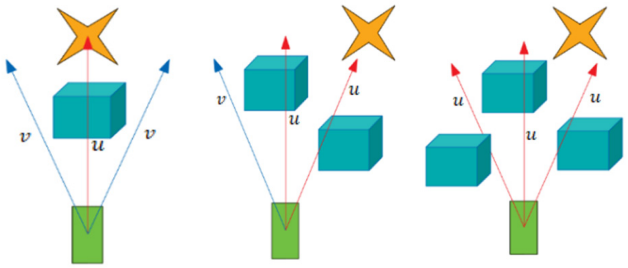

A B C

Fig. 10. An example of the three scenarios that could occur using three distance sensors.

3.3 Determining the driving direction

The direction of the movement of a vehicle can be implemented in several ways. For the purpose of this research, three were implemented one of which was finally selected as the most optimal for this model. Diagrams of all three concepts are presented in the graphic in Fig. 11.

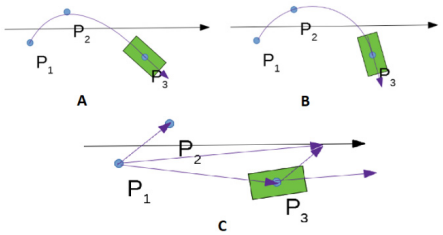

Fig. 11. Three approaches to determining the trajectory of motion A – polynomial, B – circle and C – the sum of the vectors.

Three approaches can be observed: the first (depicted in the graphic as A) was based on the second-degree polynomial (11)

$$y = ax^2 + bx + c \tag{11}$$

which was expressed for points (P_1, P_2, P_3). Although this approach was a good representation of straight-line travel and slight deviations of the UWB system, in the case of turns, it generated a significant error. The second approach (B) was to try to use the arc of the circle that was determined by the last two points and the current point. The circle equation is given as (12) and the points as (13).

$$Ax^2 + Ay^2 + Bx + Cy + D = 0 \tag{12}$$

$$P_1(x_1, y_1), P_2(x_2, y_2), P_3(x_3, y_3) \tag{13}$$

This solution proved to be very good for driving on a curve, but it was completely useless when driving on a straight line. The third approach (in the graphic as C), which was finally applied in the publication, was the direction that was determined by the vector $(\vec{u})$ as a result of the sum of the vectors that were created by the three vehicle positions that had previously been crossed (14), (15).

$$P_1(x_1, y_1), P_2(x_2, y_2), P_3(x_3, y_3), P_i(x_i, y_i) \tag{14}$$

where P_1, P_2 and P_3 are points that had previously been crossed and P_i is a current point.

$$\overrightarrow{P_3P_2} + \overrightarrow{P_3P_1} + \overrightarrow{P_3P_i} = \vec{u} \tag{15}$$

Then, a comparison between the computed u vector and the target v was made as is shown in section 3.1.

3.4 Directional tolerance

Based on the designated vector that led to the target point, the insensitivity tunnel was determined. Its task was to make the system resistant to sudden changes in the direction of motion, which resulted from the imperfections of the UWB system. In order to determine this, an insensitive area in which the readings from the UWB system could be located around the vector that connected the current point (in fact the vector from the correction) with the target point.

This value was predicted as the static Pd of the UWB system (as a result of the static measurement of the vehicle position by the UWB subsystem). A position correction was only made when the position was outside of the zone designated in this way after the aggregation into the measuring buckets. An example of such an operation is shown in Fig. 12

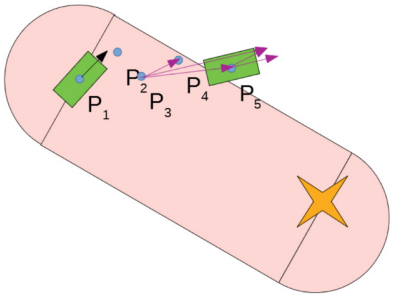

Fig. 12. An example of a correction that was made after leaving the track (in point P5) when the star was a checkpoint.

The green rectangle shows the vehicle in position P_1 – the beginning of the movement and P_5 – after aggregating four consecutive points. Points P_2, P_3 and P_4 are the intermediate positions from which the vectors led to P_5. The oval coloured area is the insensitive zone (k = 15 cm around the line from the start to end positions) and the destination symbol is marked with the star.

As long as the object was in the designated area, the algorithm assumed that it moved in the correct direction. After reaching point P5, the direction of the movement of the object was determined (based on the direction of the sum of the three previous motion vectors – $\overrightarrow{P_2P_3}, \overrightarrow{P_2P_4}$ and $\overrightarrow{P_2P_5}$ respectively). Then, the vector that was generated was oriented relative to the target point (as in 3.1 part), the correction of the driving path that had to be made was determined at the new insensitivity tunnel (based on the Pd of the UWB data) was created in line with the new track.

The relationship between the UWB acquisition frequency (Pf), turning radius (r) and vehicle speed (v) is shown in Fig. 13.

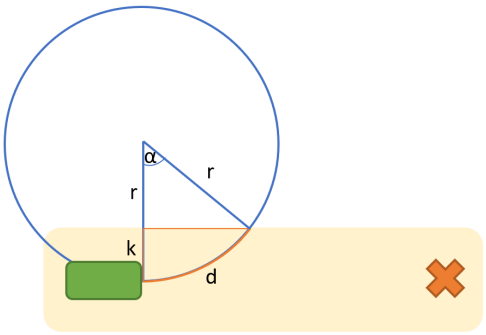

Fig. 13. Distance required to leave the insensitive zone.

When the maximum steering radius of the chassis was assumed, the section of the arc it when it left the zone was 47.1 cm. When the maximum speed of 1.1 m/s was assumed, then the vehicle left the area in 0.79 s. Taking into account a data acquisition frequency of 62.5 Hz, the vehicle should have left the zone after approximately 27 data samples – STL (samples to leave) as is shown in (16).

$$STL = \left(\frac{\cos^{-1}\left(\frac{r-k}{r}\right)}{180} * \pi * r \right) * \frac{1}{v} * P_f \tag{16}$$

A specific filtration could have changed the estimated parameters, which would have led to a higher speed, minimum radius or the positioning accuracy.

4. TESTS AND RESULTS

Based on the test platform that was constructed, tests were carried out to validate its compliance with the assumptions. For this purpose, three test scenarios were prepared and five series were carried out for three different speed variants (40%, 50% and 60% of the maximum engine power, respectively). For all of the series and speeds, the insensitivity around the path was set to 15 cm based on the Pd parameter. The test scheme is shown in Fig. 14.

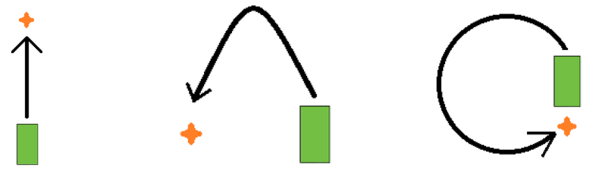

A
drive straight ahead distance of 210 cm

B
point on the side of the vehicle at a distance of 100 cm

C
point behind the vehicle at a distance of 30 cm

Fig. 14. Diagram showing the three presented research scenarios A – moving in a straight line, B – a point next to it and C – run around the circle and stop behind the starting position.

The first of the tests (presented as A on the graphics) consisted of moving in a straight line through the study area (210 cm). As part of this test, whether the vehicle was approaching the designated point and at what distance it stopped checked. The second (as in B) checked the ability of the vehicle to turn back to a point on the vehicle's starting line after any arc that was specified by the algorithm itself. The last test (shown on the graphics as C) was to run around the circle and stop behind the starting position.

As an example, the result of the data from the first measurement series, which consisted of the straight-line journeys is presented in Table 4. It contains the average results of three trips on a straight line for different engine power and their standard deviations, which clearly indicated an increase in the speed (less precision in approaching the point). It is worth noting that for each measurement series, all of the tests were completed successfully, which means that the vehicle achieved its goal without deviating from the course (which was not possible before making the modifications to the vehicle structure that were explained in the section 2)

Table 4. Measurement results for the first measurement series. Distances and standard deviation.

Engine power [%]	The average distance from the point in the series [cm]	The average standard deviation of the distance from the point in the series [cm]
40	24,8	3,2
50	16,1	7,2
60	23,8	8,9

The average distance results for all of the measurement series for three different track variants are presented in Table 5.

Table 5. Mean distance of vehicle stops from the destination point depending on the scenario.

Drive scenario	The average distance from the point for the scenario [cm]
1 – Straight line	21,5
2 – Side point	23,5
3 – Turn back point	29,6

In the table, it can be seen that as the complexity of the manoeuvre increased, the distance to stop from the target point also increased. All of the series had their insensitivity around the path set to 15 cm – the maximum distance between two points around the car (actual vs. measured) was 30cm, which, in fact, was the size of the car, and therefore each of the scenarios ended successfully. For all of the correctly completed series, it can also be noticed that the standard deviation increased with increasing speed. This shows that the series with the greater complexity of movement had the highest average distance from the point because its speed of travel was the lowest, which made the system's response time the highest. The authors observed that the results of the test could have had an impact on the results (small tires, floor, dust particles). To achieve even more accurate results, it would be worth fusing the data using data from, for example, discrete time-position sensors (Puglisi, 2015) or IMU integration (Barnea et al., 2011).

5. CONCLUSIONS

The conducted research utilized a fast prototyping platform such as LEGO Mindstorms with a UWB positioning system for navigation purpose. The analyses that were performed and are in the paper show how chassis construction constraints can affect the UWB positioning accuracy. An exemplary chassis was developed with Lego Mindstorms under specific requirements such as vehicle speed, turning radius and stopping distance. The experiments proved that with an appropriately selected insensitivity zone, it is possible to move around and a car will reach the specified point based solely on the position that can be obtained from a superior UWB system. The chassis that was created enabled the correlation between the frequency of the acquired position (UWB) and the functional parameters of the platform such as speed or turning radius to be determined, which leads to a custom adjustment towards to individual requirements.

Further research will be conducted in order to create a navigation scheme for higher speeds using another communication channel and creating a test scenario for tracking objects using multiple sensors.

ACKNOWLEDGEMENTS

This work was supported by the Ministry of Science and Higher Education of Poland funding for statutory activities.

REFERENCES

Aalto, L., Göthlin, N., Korhonen, J., & Ojala, T. (2004). Bluetooth and WAP Push Based Location-aware Mobile Advertising System. Proceedings of the 2Nd International Conference on Mobile Systems, Applications, and Services, 49–58. https://doi.org/10.1145/990064.990073

Abdel-Rahim Ahmed, Chang Kevin, & Zender Riannon. (2018). Evaluation of Vehicle Detection Systems for Traffic Signal Operations. Journal of Transportation Engineering, Part A: Systems, 144(2), 04017075. https://doi.org/10.1061/JTEPBS.0000112

Albaidhani, A., Morell, A., & Vicario, J. L. (2019). Anchor selection for UWB indoor positioning. Transactions on Emerging Telecommunications Technologies, 30(6), e3598. https://doi.org/10.1002/ett.3598

Barnea, A., Berrabah, S. A., Oprisan, C., & Doroftei, I. (2011). IMU (Inertial Measurement Unit) Integration for the Navigation and Positioning of Autonomous Robot Systems. Journal of Control Engineering and Applied Informatics, 13(2), 38-43–43.

Bayraktar Mehmet Emre, Arif Farrukh, Ozen Halit, & Tuxen Gorm. (2015). Smart Parking-Management System for Commercial Vehicle Parking at Public Rest Areas. Journal of Transportation Engineering, 141(5), 04014094. https://doi.org/10.1061/(ASCE)TE.1943-5436.0000756

Bernardin, K., & Stiefelhagen, R. (2008). Evaluating Multiple Object Tracking Performance: The CLEAR MOT Metrics. EURASIP Journal on Image and Video Processing, 2008(1), 246309. https://doi.org/10.1155/2008/246309

Biswas, J., & Veloso, M. (2010, May). WiFi localization and navigation for autonomous indoor mobile robots. 4379–4384. https://doi.org/10.1109/ROBOT.2010.5509842

Bucher, R., & Misra, D. (2002). A Synthesizable VHDL Model of the Exact Solution for Three-dimensional Hyperbolic Positioning System [Research article]. https://doi.org/10.1080/1065514021000012129

Cantón Paterna, V., Calveras Augé, A., Paradells Aspas, J., & Pérez Bullones, M. A. (2017). A Bluetooth Low Energy Indoor Positioning System with Channel Diversity, Weighted Trilateration and Kalman Filtering. Sensors, 17(12), 2927. https://doi.org/10.3390/s17122927

Combain Mobile AB. (n.d.). CPS – Combain Positioning Service. Retrieved July 8, 2017, from Wifi Positioning | Wifi Location | Cell ID – Combain website: https://combain.com

Constandache, I., Bao, X., Azizyan, M., & Choudhury, R. R. (2010). Did You See Bob?: Human Localization Using Mobile Phones. Proceedings of the Sixteenth Annual International Conference on Mobile Computing and Networking, 149–160. https://doi.org/10.1145/1859995.1860013

Education, L. (n.d.). Autonomous Parking – EV3 Coding Activities – Lesson Plans – LEGO Education. Retrieved February 1, 2019, from https://education.lego.com website: https://education.lego.com/en-us/lessons/mindstorms-ev3/autonomous-parking

Fischer, G., Dietrich, D., & Winkler, F. (2004, January). Bluetooth indoor localization system. Retrieved from https://www.researchgate.net/publication/228569802_Bluetooth_indoor_localization_system

Gesu, V. D., Lenzitti, B., Bosco, G. L., & Tegolo, D. (2000). A distributed architecture for autonomous navigation of robots. Proceedings Fifth IEEE International Workshop on Computer Architectures for Machine Perception, 190–194. https://doi.org/10.1109/CAMP.2000.875977

Gezici, S., & Poor, H. V. (2009). UWB Localization Algorithms. In Short-Range Wireless Communications (pp. 73–84). https://doi.org/10.1002/9780470740125.ch10

Grzechca, D., & Hanzel, K. (2018). The positioning accuracy based on the UWB technology for an object on circular trajectory. International Journal of Electronics and Telecommunications, 64(4), 487–494.

Grzechca, D., Hanzel, K., & Paszek, K. (2018, February). Accuracy analysis for object positioning on a circular trajectory based on the UWB location system. 69–74. https://doi.org/10.1109/TCSET.2018.8336158

Grzechca, D., Pelczar, P., & Chruszczyk, Ł. (2016). Analysis of Object Location Accuracy for iBeacon Technology based on the RSSI Path Loss Model and Fingerprint Map. International Journal of Electronics and Telecommunications, 62(4), 371–378.

Grzechca, D., Tokarz, K., Paszek, K., & Poloczek, D. (2017). Using MEMS Sensors to Enhance Positioning When the GPS Signal Disappears. Computational Collective Intelligence, 260–271. https://doi.org/10.1007/978-3-319-67077-5_25

Guo, H., Uradzinski, M., Yin, H., & Yu, M. (2015). Indoor positioning based on foot-mounted IMU. Bulletin of the Polish Academy of Sciences Technical Sciences, 63(3), 629–634. https://doi.org/10.1515/bpasts-2015-0074

Ilas, C., Rosner, D., Tataroiu, R., & Surpateanu, A. (2012). Wireless Sensors and Actuators Networks: Localization for Medical and Robotics Applications. Journal of Control Engineering and Applied Informatics, 14(2), 34-39–39.

Israel, A., & Dehy, R. (2004, Q1). INFRARED TRACKING SYSTEM.

Jin, M., Fu, C., Yu, C., & Lai, H. (2008). I 3 BM Zigbee Positioning Method for Smart Home Applications. International Journal of Smart Home.

Jurisica, L., Vitko, A., Duchon, F., & Kastan, D. (2010). Statistical approach to GPS positioning of mobile robot. Journal of Control Engineering and Applied Informatics, 12(2), 44-51–51.

Kato, H., & Billinghurst, M. (1999). Marker tracking and HMD calibration for a video-based augmented reality conferencing system. 85–94. https://doi.org/10.1109/IWAR.1999.803809

Kolakowski, J., Cichocki, J., Makal, P., & Michnowski, R. (2010). An Ultra-Wideband System for Vehicle Positioning. International Journal of Electronics and Telecommunications, 56(3), 247–256. https://doi.org/10.2478/v10177-010-0032-1

Liu, F., Chen, C., Kao, Y., Hong, C., & Yang, C. (2017). Improved ZigBee module based on fuzzy model for indoor positioning system. 2017 International Conference on Applied System Innovation (ICASI), 1331–1334. https://doi.org/10.1109/ICASI.2017.7988150

Ni, L. M., Liu, Y., Lau, Y. C., & Patil, A. P. (2004). LANDMARC: Indoor Location Sensing Using Active RFID. Wireless Networks, 10(6), 701–710. https://doi.org/10.1023/B:WINE.0000044029.06344.dd

Pescaru, D., & Curiac, D.-I. (2014). Anchor Node Localization for Wireless Sensor Networks Using Video and Compass Information Fusion. Sensors, 14(3), 4211–4224. https://doi.org/10.3390/s140304211

Pinto, M., Moreira, A. P., & Matos, A. (2012). Localization of Mobile Robots Using an Extended Kalman Filter in a LEGO NXT. IEEE Transactions on Education, 55(1), 135–144. https://doi.org/10.1109/TE.2011.2155066

Puglisi, L. J. (2015). On the Velocity and Acceleration Estimation from Discrete Time-Position Signal of Linear Encoders. Journal of Control Engineering and Applied Informatics, 17(3), 30-40–40.

Röhrig, C., Kirsch, C., Lategahn, J., Müller, M., & Telle, L. (2012). Localization of autonomous mobile robots in a cellular transport system. Engineering Letters, 20(2), 5. Retrieved from Scopus.

ScenSor Module DWM1000 – WSN | DecaWave. (n.d.). Retrieved October 19, 2017, from https://www.decawave.com/products/dwm1000-module

Stevenson, D. E., & Schwarzmeier, J. D. (2007). Building an autonomous vehicle by integrating lego mindstorms and a web cam. Proceedinds of the 38th SIGCSE Technical Symposium on Computer Science Education – SIGCSE '07, 165. https://doi.org/10.1145/1227310.1227370

Wang, X., Xu, K., & Li, Z. (2017). SmartFix: Indoor Locating Optimization Algorithm for Energy-Constrained Wearable Devices [Research article]. https://doi.org/10.1155/2017/8959356

Yang, P., Wu, W., Moniri, M., & Chibelushi, C. C. (2013). Efficient Object Localization Using Sparsely Distributed Passive RFID Tags. IEEE Transactions on Industrial Electronics, 60(12), 5914–5924. https://doi.org/10.1109/TIE.2012.2230596

Yu Wooyeon, Park SeJoon, Kim David S., & Ko Sung-Seok. (2015). Arterial Road Incident Detection Based on Time-Moving Average Method in Bluetooth-Based Wireless Vehicle Reidentification System. Journal of Transportation Engineering, 141(3), 04014084. https://doi.org/10.1061/(ASCE)TE.1943-5436.0000748

Zhao, S., Chen, Y., & Farrell, J. A. (2016). High-Precision Vehicle Navigation in Urban Environments Using an MEM's IMU and Single-Frequency GPS Receiver. IEEE Transactions on Intelligent Transportation Systems, 17(10), 2854–2867. https://doi.org/10.1109/TITS.2016.2529000